Nano Res. 2011, 4(4): 385–392
DOI 10.1007/s12274-011-0093-1
Research Article

ISSN 1998-0124
CN 11-5974/O4

Massless and Massive Particle-in-a-Box States in Single- and Bi-Layer Graphene

Sungjae Cho and Michael Fuhrer (✉)

Department of Physics and Center for Nanophysics and Advanced Materials, University of Maryland, College Park, Maryland 20742, USA

Received: 22 November 2010 / Revised:15 December 2010 / Accepted: 16 December 2010

ABSTRACT

Electron transport through short, phase-coherent metal–graphene–metal devices occurs via resonant transmission through particle-in-a-box-like states defined by the atomically-sharp metal leads. We study the spectrum of particle-in-a-box states for single- and bi-layer graphene, corresponding to massless and massive two-dimensional (2-D) fermions. The density of states D as a function of particle number n shows the expected relationships $D(n) \sim n^{1/2}$ for massless 2-D fermions (electrons in single-layer graphene) and $D(n) \sim$ constant for massive 2-D fermions (electrons in bi-layer graphene). The single parameters of the massless and massive dispersion relations are found, namely Fermi velocity $v_F = 1.1 \times 10^6$ m/s and effective mass $m^* = 0.032\, m_e$, where m_e is the electron mass, in excellent agreement with theoretical expectations.

KEYWORDS

Fabry–Perot, interference, ballistic, density of states, phase-coherent

The problem of a wavelike particle confined to a hard-walled box is one of the most basic problems in quantum mechanics. The spectra of the particle-in-a-box are strikingly different for massive and massless particles: massless particles (e.g., photons) have energies which depend linearly on quantum number, while the energies of massive particles (e.g., free electrons) depend quadratically on quantum number. For fermions in two dimensions this leads to a density of single-particle states $D \equiv \mathrm{d}n/\mathrm{d}E$, where E is the particle energy and n the particle density, which varies as the square root of particle density, i.e., $D(n) \sim n^{1/2}$, for massless particles, and is independent of particle density for massive particles, i.e., $D(n) \sim$ constant. Here we show that mesoscopic, ballistic [1–3] single-layer [4, 5] and bi-layer [6, 7] metal–graphene–metal devices act as Fabry–Perot cavities for electrons confined between the atomically-sharp partially-reflective metal leads. Electronic conduction occurs through resonant states of the Fabry–Perot cavity, which are exactly analogous to the particle-in-a-box states of an electron confined by perfectly reflective walls. $D(n)$ is measured, and the expected dependences on particle number are verified: $D \sim n^{1/2}$ for massless particles in single-layer graphene, and $D \sim$ constant for massive particles in bi-layer graphene. $D(n)$ is used to extract the single constants in the dispersion relations: the Fermi velocity $v_F = 1.09 \times 10^6$ m/s for massless particles in single-layer graphene [4, 5], and the effective mass $m^* = 0.032\, m_e$, where m_e is the electron mass, for massive particles in bi-layer graphene [6, 7] in excellent agreement with theoretical expectations [6, 8–11] and other experimental

Address correspondence to mfuhrer@umd.edu

results [4, 5, 12–14].

We first review the results of the two-dimensional (2-D) particle-in-a-box problem. Figures 1(a) and 1(b), illustrate the massless and massive dispersion relations respectively

$$E = \hbar v_F |\boldsymbol{k}| \quad \text{(massless)} \tag{1a}$$

$$E = \frac{\hbar^2 k^2}{2m^*} \quad \text{(massive)} \tag{1b}$$

where $\hbar = h/2\pi$, and h is Planck's constant; each dispersion relation is characterized by a single parameter, m^* for the massive dispersion, and v_F for the massless dispersion. For particles confined to a 2-D box of width W and length L the hard-wall boundary condition quantizes the wavevector $\boldsymbol{k} = (k_x, k_y) = (\pi p/L, \pi q/W)$ resulting in two positive quantum numbers p, q. Figures 1(c) and 1(d) illustrate this quantization, where each point represents an allowed wavevector. Then the energies in terms of quantum numbers are given by the familiar relations $E = \hbar v_F \pi \sqrt{(p/W)^2 + (q/L)^2}$ (massless) and $E = (h^2/8m)[(p/W)^2 + (q/L)^2]$ (massive). For fermions at zero temperature, the occupancy of a particle-in-a-box state will be the degeneracy of individual states g for state of energy $E < E_F$ (the Fermi energy) and zero for states $E > E_F$. The number of states with $E < E_F$ is given by $N = gk_F^2 WL/4\pi$, where $k_F \equiv k(E_F)$ is the Fermi wavevector. Figures 1(c) and 1(d) illustrate the occupied states included for equally-spaced values of E_F, and Figs. 1(e) and 1(f) show the energies of the particle-in-a-box states as a function of particle number N for massless and massive 2-D fermions respectively.

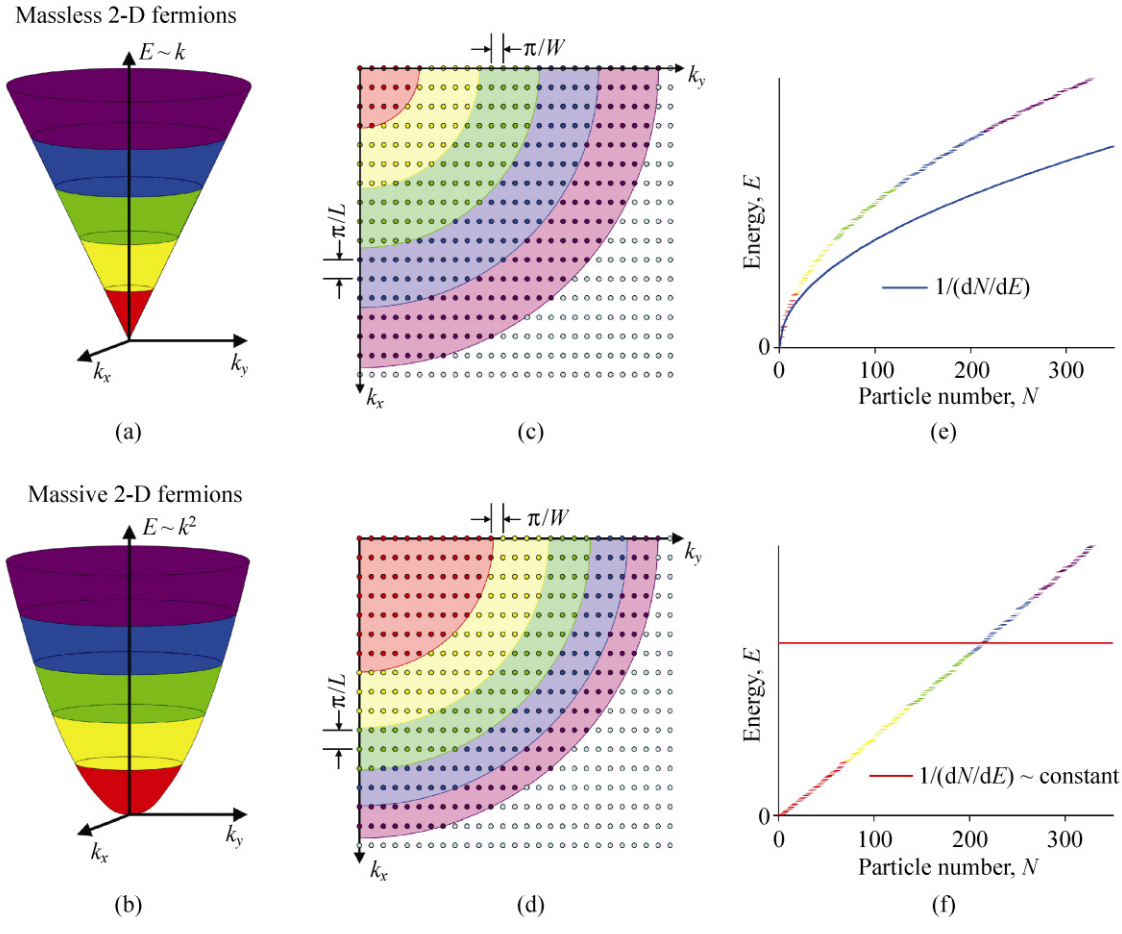

Figure 1 (a) Massless dispersion and (b) massive dispersion relations in two dimensions. (c–d) Allowed wavenumbers for a particle in a box of aspect ratio $W/L = 1.6$. Solid lines are contours of equal energy for massless dispersion relation (c) and for massive dispersion relation (d). (e–f) Particle energy as a function of particle number in a box with $W/L = 1.6$ for massless dispersion relation (e) and for massive dispersion relation (f)

The linear and square-root dependences of $E(N)$ for massless and massive 2-D fermions respectively are evident in Figs. 1(e) and 1(f).

Using the areal density of particles $n = N/WL = gk_F^2/4\pi$ we then have the following relations for the dependences of the Fermi energy E_F and density of states D on density

$$E_F = \hbar v_F \sqrt{\pi n} \quad \text{(massless)} \tag{2a}$$

$$E_F = \frac{\pi \hbar^2 n}{2m^*} \quad \text{(massive)} \tag{2b}$$

$$D = \frac{1}{\hbar v_F}\sqrt{\frac{gn}{\pi}} \quad \text{(massless)} \tag{3a}$$

$$D = \frac{gm^*}{2\pi\hbar^2} \quad \text{(massive)} \tag{3b}$$

Thus the measurement of D as a function of n distinguishes massive and massless particles, and (given knowledge of the degeneracy g) also determines the constants of the dispersion relations v_F and m^*.

Single- and bi-layer graphene may be used to realize the dispersion relations in Eqs. (3a) and (3b) as follows. Single-layer graphene is well-described by a tight-binding model considering only the π-orbitals at each atomic site. At zero doping, the π and π* bands meet at two points in the Brillouin zone with wavevector $\boldsymbol{K}$. This crossing is preserved as long as the two atoms A and B in the unit cell are equivalent. Taking $E(\boldsymbol{K}) = 0$, and measuring k away from the $\boldsymbol{K}$ point, the band structure is well-approximated by Eq. (1a), with $v_F = (\sqrt{3}/2)a\gamma_0/\hbar \approx 1.0 \times 10^6$ m/s where $a = 2.46$ Å is the graphene lattice constant and $\gamma_0 \approx 3.16$ eV [15] is the nearest-neighbor hopping parameter. In Bernal-stacked bi-layer graphene [6–10] atom A in one layer is stacked above atom B′ in the 2nd layer, and this A–B′ coupling breaks the AB equivalency of the graphene unit cell and results in two bands which may be approximated as hyperbolic

$$E_{\pm}(k) = \pm\left[\sqrt{(\hbar v_F k)^2 + \gamma_1^2/4} - \gamma_1/2\right] \text{[8]}$$

where $\gamma_1 \approx 0.4$ eV [16] is the inter-layer (A–B′) hopping parameter. At $k = 0$ the effective mass is given by $m^* = \gamma_1/2v_F^2 \approx 0.03\, m_e$. In both single- and bi-layer graphene the degeneracy $g = 4$, due to the two-fold spin degeneracy and the two-fold valley degeneracy (presence of two $\boldsymbol{K}$ points).

We now discuss the graphene samples used in this study. We mechanically exfoliated Kish graphite on 300 nm SiO_2/Si substrates to obtain single and bi-layer graphene [4, 5, 7]. Single-layer graphene is more transparent than two- or more- layer graphene under an optical microscope as seen in Fig. 2. After locating graphene flakes, Cr/Au (5 nm/50 nm) electrical contacts were thermally deposited. The channel lengths L for Fabry–Perot interference measurement were 200–300 nm as measured by a scanning electron microscope. The maximum field-effect mobilities at low temperature estimated from the four-probe resistivity of the adjacent graphene sections were 15 000 cm²/(V·s) and 4000 cm²/(V·s) for single- and bi-layer graphene respectively. Figures 2(a) and 2(b) show completed single- and bi-layer graphene devices respectively. Electrodes were patterned on each graphene flake to form a large-area Hall-bar arrangement for characterizing the longitudinal and Hall conductivities (σ_{xx} and σ_{xy}) of the sample. In addition, closely-spaced (150–300 nm) electrode pairs form Fabry–Perot cavities on the same sample. Figures 2(c) and 2(d) show σ_{xx} and σ_{xy} for the single- and bi-layer graphene devices shown in Figs. 1(a) and 1(b), respectively, measured in high magnetic field (9 T) and as a function of back-gate voltage V_g, which controls the carrier density $n = c_g V_g/e$, where $c_g = 1.1 \times 10^{-8}$ F/cm^{-2}, and e is the electronic charge. The quantized Hall effect (QHE) is evident as plateaux with $\sigma_{xy} = \nu e^2/h$, and corresponding minima in σ_{xx}. Berry's phases of π and 2π lead to QHE in single- and bi-layer graphene at filling factors $\nu = 4(i + 1/2)$ and $4(i + 1)$, where i is an integer [4, 5, 7], thus our observation of the half-integer and full-integer QHE confirms the identification of these samples as single- and bi-layer graphene respectively.

Figures 2(e) and 2(f) show the two-probe conductances as a function of gate voltage $G(V_g)$ for Fabry–Perot cavities on the single- and bi-layer devices, respectively, at zero magnetic field. We shift the curves horizontally by an amount V_D which we identify as the gate voltage at which the Fermi level lies closest to the Dirac point. The conductance rises away from $V_g - V_D = 0$ as observed by previously [4, 5, 7]. Small

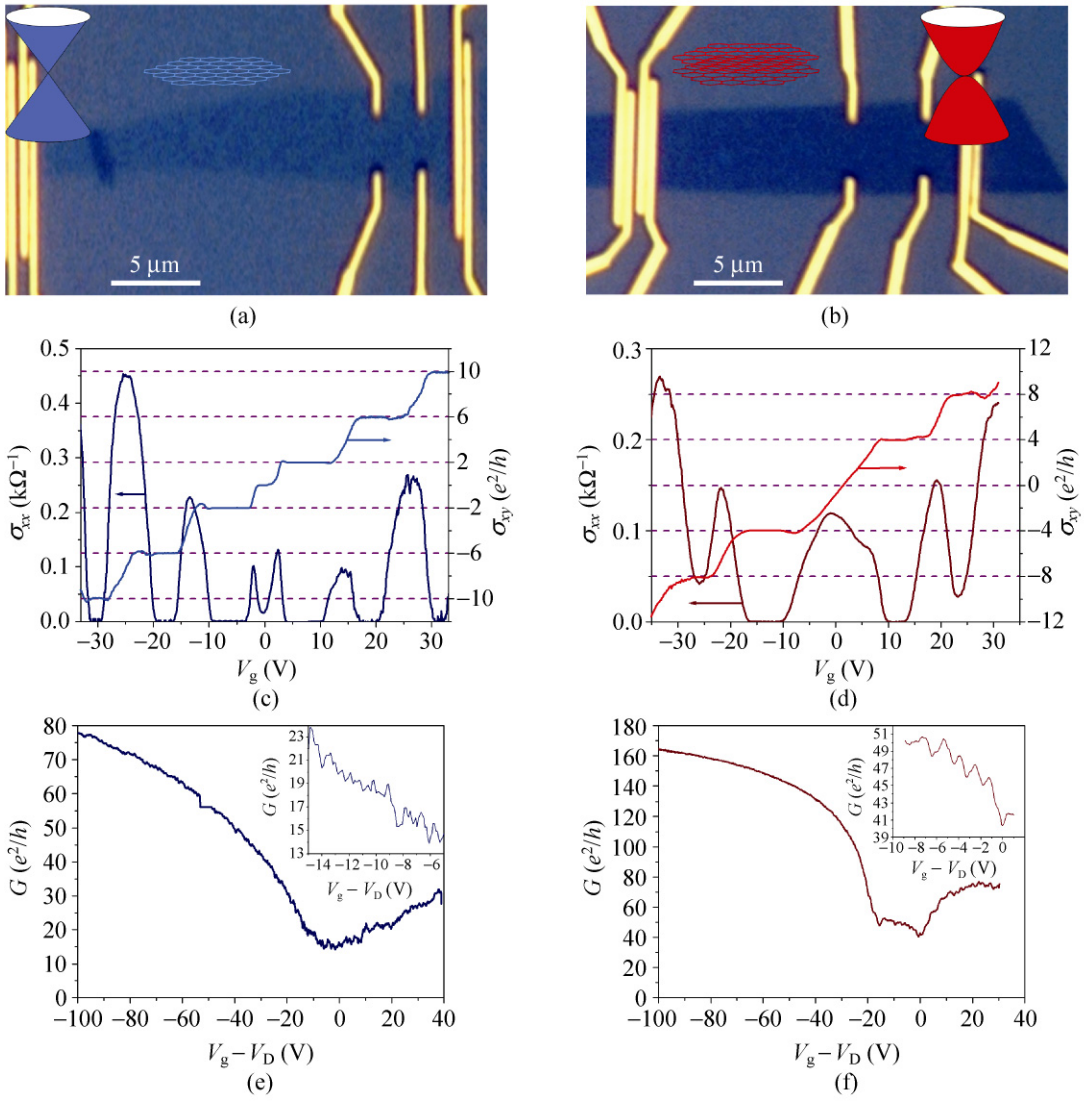

Figure 2 Optical micrographs of a single-layer graphene device (a) and a bi-layer graphene device (b). Longitudinal and Hall conductivity as a function of gate voltage at a magnetic field of 9 T and temperature of 1.3 K for a single-layer graphene device (c) and a bi-layer graphene device (d). Two-probe conductance as a function of gate voltage at zero magnetic field and temperature of 1.3 K for a single-layer graphene device (e) and a bi-layer graphene device (f)

reproducible fluctuations of the conductance with magnitude of order e^2/h can be seen (see insets to Figs. 2(e) and 2(f)); these fluctuations are not universal conductance fluctuations but, as argued below, result from the interference of ballistic electron waves in the Fabry–Perot cavity [1, 2].

Figure 3 shows color-scale maps of the differential conductance dI/dV as a function of bias voltage V applied between the two electrical contacts and gate voltage V_g for the single- and bi-layer devices shown in Fig. 2. A pattern of diagonal lines of increased conductance is evident; this pattern is the signature of Fabry–Perot interference in a mesoscopic device [1, 2, 17]. Neighboring diagonal lines have similar slopes, and diagonal lines of similar positive and negative slope are found in each V_g region. Each individual diagonal line results from the enhancement in conductance when a particle-in-a-box resonance, or a group of constructively-interfering resonances, is aligned with the source electrode (+V) or drain electrode (–V); the symmetry about $V = 0$ reflects the source-drain symmetry of the device. Note that the

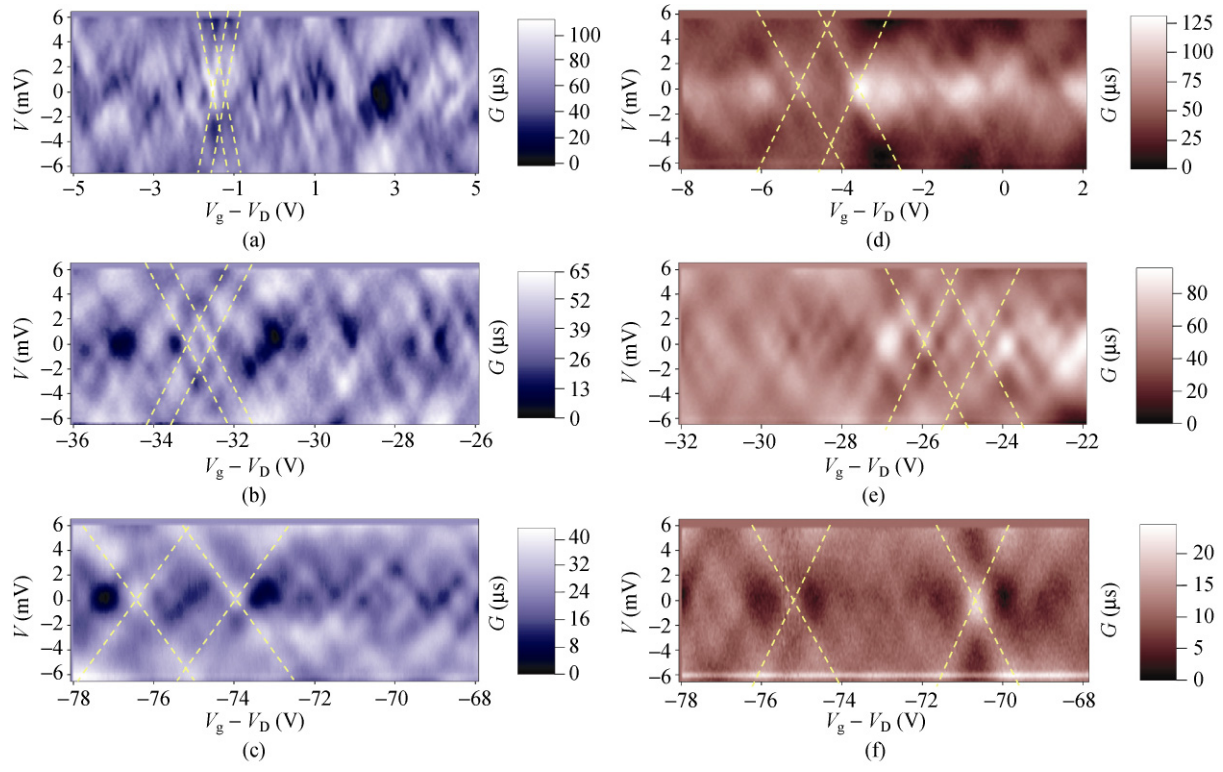

Figure 3 Color-scale 2-D plots of differential conductance $G = dI/dV$ as a function of bias voltage V and gate voltage V_g measured in single (a)–(c) and bi-layer (d)–(f) graphene at temperature $T = 1.3$ K. A smooth background conductance was subtracted to enhance the patterns. The sample dimensions are 1.5 μm (W) × 0.3 μm (L) for single-layer graphene and 4.3 μm (W) × 0.2 μm (L) for bi-layer graphene. Yellow lines illustrate the slope of the Fabry–Perot resonances

pattern is inconsistent with Coulomb blockade; there are no diamond-shaped low conductance regions around $V = 0$, and the conductance is comparable to or greater than e^2/h, ruling out Coulomb blockade.

Resonant transmission through a Fabry–Perot cavity has been reported previously for carbon nanotubes (CNTs) [17, 18] and graphene [1, 2]. In the case of CNTs, there is a single path length L connecting the electrodes, and the resonances are evenly spaced in V and V_g.

In graphene [1, 2], the resonances are randomly spaced, which may result from a spread of path lengths due to non-parallel electrodes or electron paths which are not perpendicular to the electrode–graphene interfaces. In Ref. [2], the splitting of resonances in a magnetic field was used to measure the g factor as well as the density of states for single-layer graphene. However, important information can also be gained by analyzing the slope $\Delta V/\Delta V_g$ of the resonant lines in Fig. 3. Briefly, the slope measures the change in energy $\Delta E = e\Delta V/2$ (the factor of two results from the potentials $+\Delta V/2$ and $-\Delta V/2$ applied to the two electrodes relative to the graphene in a ballistic device) of the resonance as the particle number $dn = c_g\Delta V_g/e$ is changed. The slope is then equal to $\Delta V/\Delta V_g = (2c_g/e^2)\Delta E/\Delta n = (2c_g/e^2)D^{-1}$; i.e., the slope is inversely proportional to the density of states. From Eqs. (3a) and (3b) above, we expect that $\Delta V/\Delta V_g \sim n^{-1/2} \sim |V_g - V_D|^{-1/2}$ for the single-layer (massless dispersion) sample, and $\Delta V/\Delta V_g \sim$ constant for the bi-layer (massive dispersion) sample. Figures 3(a)–3(c) show that the slope indeed varies significantly with gate voltage (electron density) for the single-layer graphene sample, with the highest slope occurring near $V_g - V_D = 0$. The slope is nearly constant in the bi-layer graphene sample (Figs. 3(d)–3(f)).

Figure 4 plots the density of states $D = (e^2/2c_g) \times (\Delta V/\Delta V_g)^{-1}$ for the single- and bi-layer graphene samples extracted from Figs. 3(a)–3(f) and additional data (not shown) as a function of electron density $n = c_g(V_g - V_D)/e$. Data from an additional single-layer sample are also

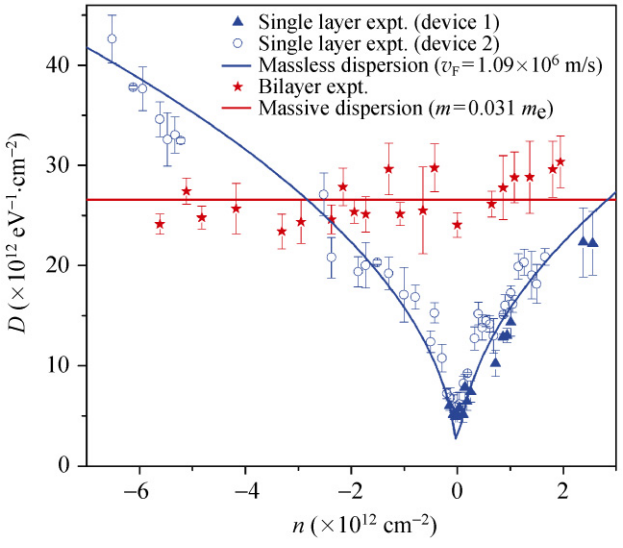

Figure 4 Density of states of single-layer graphene (blue symbols; data from two devices shown) and bi-layer graphene (red symbols, data from one device shown) as a function of particle density. Solid lines are fits to Eq. (3a) (blue) with $v_F = 1.09 \times 10^6$ m/s and Eq. (3b) (red) with $m^* = 0.032\ m_e$

shown. Solid lines are fits to Eqs. (3a) and (3b) for the single-layer and bi-layer data respectively. The expected dependences on particle number are verified: $D \sim n^{1/2}$ for massless particles in single-layer graphene (Eq. (3a)), and $D \sim constant$ for massive particles in bi-layer graphene (Eq. (3b)). Only a single fitting parameter is used in each fit, $v_F = (1.09 \pm 0.01) \times 10^6$ m/s for massless particles in single-layer graphene and $m^* = (0.0315 \pm 0.0001) m_e$ for massive particles in bi-layer graphene. As discussed in detail below, the parameter for single-layer graphene is in excellent agreement with theoretical and other experimental results, but the constant effective mass for bi-layer graphene up to $n \sim 5.5 \times 10^{12}$ /cm^2 is surprising [8, 19, 20].

We now discuss the detailed dependence of the density of states on particle number in single- and bi-layer graphene, and the implications of the results for understanding the electronic structure of these materials. From the fit to Eq. (3a) in Fig. 4, we determine a Fermi velocity for single-layer graphene of $v_F = (1.09 \pm 0.01) \times 10^6$ m/s. A tight-binding model of graphene [21] gives $v_F = (\sqrt{3}/2) a\gamma_0/\hbar \approx 1.0 \times 10^6$ m/s where $a = 2.46$ Å is the graphene lattice constant and $\gamma_0 \approx 3.16$ eV [15] is the nearest-neighbor hopping parameter. The inclusion of electron–electron interactions will renormalize the Fermi velocity slightly [11], and the slightly higher v_F observed here is consistent with other experiments on graphene [4, 5, 22, 23].

The density of states in single-layer graphene remains finite as $n \to 0$ due to charge inhomogeneity caused by charged impurities near the graphene, as has been observed previously. The minimum density of states D on the order of 2×10^{12} eV^{-1}·cm^{-2} corresponds to a charge density n on the order of 10^{11} cm^{-2}, in agreement with theoretical [24] and experimental expectations [25, 26] for the minimum charge density at the Dirac point in the presence of charged impurity disorder due to the SiO_2 substrate.

We now discuss bi-layer graphene. From the fit to Eq. (3b) in Fig. 4, we determine $m^* = 0.032\ m_e$. Assuming $v_F = 1.09 \times 10^6$ m/s we have $\gamma_1 = 0.40$ eV, in excellent agreement with the experimental values for graphite of 0.39 eV ± 0.01 eV [27] and with other experiments on bi-layer graphene [13, 14]. Because the bands are not strictly parabolic, the density of states should depend on particle density, increasing with increasing particle density. The hyperbolic nature of the bands becomes important for particle densities roughly greater than $\gamma_1^2/(4\pi\hbar^2 v_F^2) \approx 4.4 \times 10^{12}$ cm^{-2} [8]. Experimentally, we see little variation in the density of states for particle densities up to 5.5×10^{12} cm^{-2}, indicating a wider range of validity of the parabolic spectrum than expected. We do not currently understand this discrepancy, but we note that electron–electron interactions should again be important, as was pointed out previously in the failure of the single-particle picture to quantitatively explain the cyclotron resonance spectrum in bi-layer graphene [13]. Interactions are expected to reduce the mass in bi-layer graphene, though the renormalized mass is expected to be more density-dependent, contrary to our observations [28]. Further measurement up to higher carrier density may be required to understand this discrepancy.

In conclusion, we have probed the density of particle-in-a-box states as a function of particle number for massless 2-D fermions (single-layer graphene) and massive 2-D fermions (bi-layer graphene) in phase-coherent measurement. Understanding of coherent transport is an essential step to realize other interesting experiments with graphene such as focusing lenses, Klein tunneling and graphene superlattices [29–32].

The density of states varies as the square-root of particle number for massless 2-D fermions, and is constant for massive 2-D fermions. The single parameters in the dispersion relations are extracted; the Fermi velocity $v_F = 1.1 \times 10^6$ m/s for massless particles in single-layer graphene and effective mass $m^* = 0.032\ m_e$ for massive particles in bi-layer graphene, in excellent agreement with theoretical expectations and other experimental observations.

Acknowledgements

This work has been supported by the U.S. ONR (grants Nos. N000140911064 and N000140610882), the National Science Foundation (NSF) (grant No. CCF-06-34321), and the UMD-NSF-MRSEC (grant No. DMR-05-20471). We acknowledge useful discussions with S. Adam and S. Das Sarma.

References

[1] Miao, F.; Wijeratne, S.; Zhang, Y.; Coskun, U. C.; Bao, W.; Lau, C. N. Phase-coherent transport in graphene quantum billiards. *Science* **2007**, *317*, 1530–1533.

[2] Lundeberg, M. B.; Folk, J. A. Spin-resolved quantum interference in graphene. *Nat. Phys.* **2009**, *5*, 894–897.

[3] Young, A. F.; Kim, P. Quantum interference and Klein tunnelling in graphene heterojunctions. *Nat. Phys.* **2009**, *5*, 222–226.

[4] Novoselov, K. S.; Geim, A. K.; S.; Morozov, V.; Jiang, D.; Katsnelson, M. I.; Grigorieva, I. V.; Dubonos, S. V.; Firsov, A. A. Two-dimensional gas of massless Dirac fermions in graphene. *Nature* **2005**, *438*, 197–200.

[5] Zhang, Y.; Tan, Y. W.; Stormer, H. L.; Kim, P. Experimental observation of the quantum Hall effect and Berry's phase in graphene. *Nature* **2005**, *438*, 201–204.

[6] Koshino, M.; Ando, T. Transport in bilayer graphene: Calculations within a self-consistent Born approximation. *Phys. Rev. B* **2006**, *73*, 245403.

[7] Novoselov, K. S.; McCann, E.; Morozov, S. V.; Fal'ko, V. I.; Katsnelson, M. I.; Zeitler, U.; Jiang, D.; Schedin, F.; Geim, A. K. Unconventional quantum Hall effect and Berry's phase of 2π in bilayer graphene. *Nat. Phys.* **2006**, *2*, 177–180.

[8] McCann, E.; Fal'ko, V. I. Landau-level degeneracy and quantum Hall effect in a graphite bilayer. *Phys. Rev. Lett.* **2006**, *96*, 086805.

[9] Nilson, J.; Castro Neto, A. H.; Guinea, F.; Peres, N. M. R. Electronic properties of graphene multilayers. *Phys. Rev. Lett.* **2006**, *97*, 266801.

[10] Partoens, B.; Peeters, F. M. From graphene to graphite: Electronic structure around the K point. *Phys. Rev. B* **2006**, *74*, 075404.

[11] Das Sarma, S.; Hwang, E. H.; Tse, W. K. Many-body interaction effects in doped and undoped graphene: Fermi liquid versus non-Fermi liquid. *Phys. Rev. B* **2007**, *75*, 121406.

[12] Bostwick, A.; Ohta, T.; Seyller, T.; Horn, K.; Rotenberg, E. Quasiparticle dynamics in graphene. *Nat. Phys.* **2007**, *3*, 36–40.

[13] Henriksen, E. A.; Jiang, Z.; Tung, L. C.; Schwartz, M. E.; Takita, M.; Wang, Y. J.; Kim, P.; Stormer, H. L. Cyclotron resonance in bilayer graphene. *Phys. Rev. Lett.* **2008**, *100*, 087403.

[14] Ohta, T.; Bostwick, A.; Seyller, T.; Horn, K.; Rotenberg, E. Controlling the electronic structure of bilayer graphene. *Science* **2006**, *313*, 951–954.

[15] Toy, W. W.; Dresselhaus, M. S. Minority carriers in graphite and the H-point magnetoreflection spectra. *Phys. Rev. B* **1977**, *15*, 4077–4090.

[16] Dresselhaus, M. S.; Dresselhaus, G. Intercalation compound of graphite. *Adv. Phys.* **1981**, *30*, 139–326.

[17] Liang, W.; Bockrath, M.; Bozovic, D.; Hafner, J. H.; Tinkham, M.; Park, H. Fabry–Perot interference in a nanotube electron waveguide. *Nature* **2001**, *411*, 665–669.

[18] Cao, J.; Wang, Q.; Dai, H. Electron transport in very clean, as-grown suspended carbon nanotubes. *Nat. Mater.* **2005**, *4*, 745–749.

[19] Henriksen, E. A.; Eisenstein, J. P. Measurement of the electronic compressibility of bilayer graphene. *Phys. Rev. B* **2010**, *82*, 041412.

[20] Young, A. F.; Dean, C. R.; Meric, I.; Sorgenfrei, S.; Ren, H.; Watanabe, K.; Taniguchi, T.; Hone, J.; Shepard, K. L.; Kim, P. Electronic compressibility of gapped bilayer graphene. *arXiv:1004.5556*, **2010**.

[21] Wallace, P. R. The band theory of graphite. *Phys. Rev.* **1947**, *71*, 622–634.

[22] Jiang, Z.; Henriksen, E. A.; Tung, L. C.; Wang, Y. J.; Schwartz, M. E.; Han, M. Y.; Kim, P.; Stormer, H. L. Infrared spectroscopy of Landau levels of graphene. *Phys. Rev. Lett.* **2007**, *98*, 197403.

[23] Sadowski, M. L.; Martinez, G.; Potemski, M.; Berger, C.; de Heer, W. A. Landau level spectroscopy of ultrathin graphite layers. *Phys. Rev. Lett.* **2006**, *97*, 266405.

[24] Adam, S.; Hwang, E. H.; Galitski, V. M.; Das Sarma, S. Self-consistent theory for graphene transport. *Proc. Natl. Acad. Sci. USA* **2007**, *104*, 18392–18397.

[25] Chen, J. H.; Jang, C.; Adam, S.; Fuhrer, M. S.; Williams, E. D.; Ishigami, M. Charged impurity scattering in graphene. *Nat. Phys*. **2008**, *4*, 377–381.

[26] Martin, J.; Akerman, N.; Ulbricht, G.; Lohmann, T.; Smet, J. H.; von Klitzing, K.; Yacoby, A. Observation of electron–hole puddles in graphene using a scanning single-electron transistor. *Nat. Phys*. **2008**, *4*, 144–148.

[27] Misu, A.; Mendez, E. E.; Dresselhaus, M. S. Near-infrared reflectivity of graphite under hydrostatic pressure. I. Experiment. *J. Phys. Soc. Jap.* **1979**, *47*, 199–207.

[28] Borghia, G; Polinib, M.; Asgaric, R.; MacDonald, A. H. Fermi velocity enhancement in monolayer and bilayer graphene. *Solid State Commun.* **2009**, *149*, 1117–1122.

[29] Cheianov, V. V.; Fal'ko, V. I. Selective transmission of Dirac electrons and ballistic magnetoresistance of n–p junctions in graphene. *Phys. Rev. B* **2006**, *74*, 041403.

[30] Cheianov, V. V.; Fal'ko, V.; Altshuler, B. L. The focusing of electron flow and a Veselago lens in graphene p–n junctions. *Science* **2007**, *315*, 1252–1255.

[31] Katsnelson, M. I.; Novoselov, K. S.; Geim, A. K. Chiral tunnelling and the Klein paradox in graphene. *Nat. Phys.* **2006**, *2*, 620–625.

[32] Park, C. H.; Yang, L.; Son, Y. W.; Cohen, M. L.; Louie, S. G. Anisotropic behaviours of massless Dirac fermions in graphene under periodic potentials. *Nat. Phys.* **2008**, *4*, 213–217.